

Tunable strong magnetic anisotropy in two-dimensional van der Waals antiferromagnets

Feiping Xiao¹ and Qingjun Tong^{1,*}

¹*School of Physics and Electronics, Hunan University, Changsha 410082, China*

(Dated: August 16, 2022)

We show that anisotropic energy of a 2D antiferromagnet is greatly enhanced via stacking on a magnetic substrate layer, arising from the sublattice-dependent interlayer magnetic interaction that defines an effective anisotropic energy. Interestingly, this effective energy couples strongly with the interlayer stacking order and the magnetic order of the substrate layer, providing unique mechanical and magnetic means to control the antiferromagnetic order. These two types of control methods affect distinctly the sublattice magnetization dynamics, with a change of the ratio of sublattice precession amplitudes in the former and its chirality in the later. In moiré superlattices formed by a relative twist or strain between the layers, the coupling with stacking order introduces a landscape of effective anisotropic energy across the moiré, which can be utilized to create nonuniform antiferromagnetic textures featuring periodically localized low-energy magnons.

KEYWORDS: 2D magnets, antiferromagnetic order, van der Waals heterostructure, moiré pattern

Introduction.— The demand of down scale of information carriers has spurred tremendous interest in two-dimensional (2D) layered magnets, because of their potential applications in constructing atomically thin spintronic devices [1–5]. Compared with 2D ferromagnets [6–15], antiferromagnetic (AFM) materials are more robust for information storage, owing to their immunity against external magnetic disturbance [16–23]. In addition, AFM magnets possess two degenerate elementary chargeless bosonic modes (magnons), operating at terahertz regime and allowing for ultrafast transfer of spin information [24–28]. A prerequisite for 2D AFM application is the existence of a strong and tunable magnetic anisotropy [29, 30]. First, a strong magnetic anisotropy is needed to stabilize 2D magnetism against thermal fluctuations [31], and achieve terahertz AFM resonance frequency [32]. Second, a tunable magnetic anisotropy can be utilized to manipulate AFM order, whose control is usually quite difficult due to the absence of net magnetization. This motivates the ongoing searching for 2D AFM magnets with tunable strong magnetic anisotropy.

Besides the material-determined intrinsic anisotropy, magnetic order in a ferromagnet can also be stabilized and oriented by an external magnetic field, achieving the spin polarized state (c.f. Figure 1a). In contrast, because of its staggered nature, the AFM magnetic order can only be controlled by a staggered sublattice magnetic field that points along opposite direction (c.f. Figure 1b). This requires atomic-scale magnetic control, which, however, is impracticable for conventional magnetic techniques. The recent advent of 2D van der Waals layered magnets sheds new light on this intractable problem [3, 4]. A unique advantage of van der Waals materials is the appearance of an additional degree of freedom regarding interlayer atomic registry, i.e. the vertical arrangement of atomic sites of adjacent layers [33–48]. When the AFM sublattice sits differently on a magnetic substrate layer, they would experience a distinct inter-

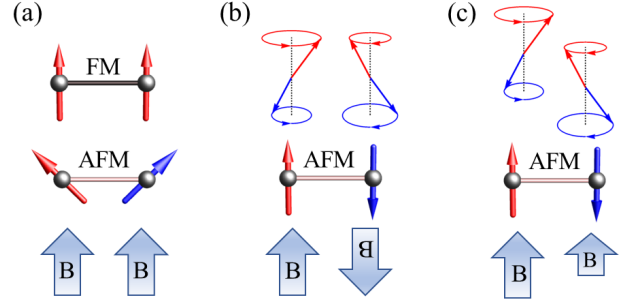


FIG. 1. Schematics of the response of magnetic orders with weak uniaxial anisotropy to different sublattice magnetic field. (a) A uniform sublattice magnetic field stabilizes the FM order, while destabilizes the AFM order into spin flop phase. (b) A staggered sublattice magnetic field pointing in opposite direction stabilizes the AFM order with two degenerate AFM resonance modes. (c) A general staggered sublattice magnetic field stabilizes the AFM order with two nondegenerate AFM resonance modes.

layer magnetic interaction. In the Landau-Lifshitz theory [49], this sublattice dependent magnetic interaction defines an effective staggered sublattice magnetic field that operating at atomic scale (c.f. Figure 1c). This staggered effective field arising from the unique stacking degree of freedom in van der Waals materials has not been considered in conventional magnetic control schemes, such as exchange bias where AFM materials are mainly used as passive pinning substrates [50]. This motivates us to explore the possibility to control AFM order in van der Waals layered 2D magnets in pursuit of tunable strong magnetic anisotropy.

Here, via stacking an AFM monolayer on a ferromagnetic (FM) substrate, we show that the interlayer magnetic interaction introduces a staggered sublattice magnetic field, which can be divided into an effective anisotropic field that stabilizes the AFM order and an effective Zeeman field that breaks the degeneracy of

magnon modes. Interestingly, the effective anisotropic field couples strongly with interlayer stacking order and magnetic order of the substrate layer, and even can change sign that flips the AFM order. These two types of couplings affect distinctly AFM magnetization dynamics, where an interlayer shift changes the ratio of sublattice precession amplitudes while a magnetic field changes its chirality. In the moiré superlattice formed by a relative twist or strain between the magnetic layers, the stacking dependent effective anisotropic field creates nonuniform magnetic textures, including AFM skyrmions. The low-energy magnons feel a trapping potential contributed from both the AFM texture and the landscape of the effective field, and are periodically trapped in the moiré. Our findings, supported by first-principles calculations on MnPS₃/CrCl₃ heterobilayer, are general in layered 2D magnets (AFM MnPS₃ homobilayer is studied in the discussion section).

Effective magnetic anisotropy and its tunability.— We first give a general analysis on how to create a tunable magnetic anisotropy from the sublattice dependent interlayer magnetic interaction. The model Hamiltonian for a commensurate bilayer consisting of an AFM top layer and an FM bottom layer is

$$H^{bi} = \sum_{\langle i,j \rangle, l} (J^l \mathbf{m}_i^l \mathbf{m}_j^l - K_0^l m_{z,i}^2) - \sum_{i,j} J_{i,j}^\perp(\mathbf{r}) \mathbf{m}_i^t \mathbf{m}_j^b(1)$$

where $\mathbf{m}_i^l = \mathbf{M}_i^l / M_0^l$ is the normalized magnetic moment at i -site of the l -th layer with M_0^l being its magnitude and J^l ($J_{i,j}^\perp$) is the intralayer (interlayer) exchange coupling. The interlayer part depends on the interlayer distance and inplane shift \mathbf{r} between the magnetic atoms of the two layers [34]. The summation of lattice sites includes the sublattice degree of freedom and runs over nearest neighbor sites $\langle i,j \rangle$ in the intralayer part. K_0^l is anisotropy energy, which is assumed to be small for the AFM top layer so that its magnetic order can be tuned.

In the Landau-Lifshitz theory, the magnetic moments of the top AFM layer at A and B sublattice feel a local effective field $\mathbf{H}_{A/B}^{eff}(\mathbf{r}) = -\partial H^{bi} / \partial \mathbf{m}_{i,A/B}$. Neglecting the exchange field that does not affect the magnetic anisotropy and assuming the FM order in the bottom layer is uniform, i.e. $\mathbf{m}_j^b = \mathbf{n}$, this field reads

$$\mathbf{H}_{A/B}^{eff}(\mathbf{r}) = \pm \tau_0 K_0^t \mathbf{z} + [\pm \tau K_{eff}(\mathbf{r}) + Z_{eff}(\mathbf{r})] \mathbf{n}, \quad (2)$$

where $\tau_0 = \text{sgn}[\mathbf{l} \cdot \mathbf{z}]$ and $\tau = \text{sgn}[\mathbf{l} \cdot \mathbf{n}]$ with the AFM Néel vector $\mathbf{l} = (\mathbf{m}_A - \mathbf{m}_B)/2$, and we have defined $K_{eff}(\mathbf{r}) = \sum_j [J_j^\perp(\mathbf{r}_A) - J_j^\perp(\mathbf{r}_B)]/2$ and $Z_{eff}(\mathbf{r}) = \sum_j [J_j^\perp(\mathbf{r}_A) + J_j^\perp(\mathbf{r}_B)]/2$. From Eq. (2), one immediately recognizes that the discrepancy of the two sublattice effective field $K_{eff}(\mathbf{r})$ acts as an effective anisotropic energy that can stabilize the AFM order. While their average $Z_{eff}(\mathbf{r})$ acts as a uniform effective Zeeman energy that can break the degeneracy of the AFM resonance modes and even lead to spin flop phase when

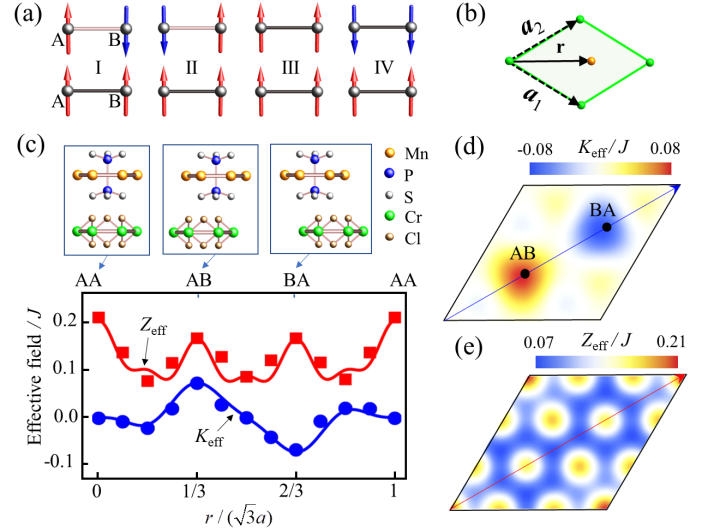


FIG. 2. (a) Four magnetic configurations used to calculate the interlayer interaction induced effective fields. (b) A shifting vector \mathbf{r} that characterizes interlayer atomic registry of a commensurate MnPS₃/CrCl₃ bilayer, which is defined in a unit cell with unit vectors $\mathbf{a}_{1/2}$. (c) First-principles calculated effective anisotropic field K_{eff} (blue dots) and Zeeman field Z_{eff} (red squares) in an AFM monolayer MnPS₃ induced by interlayer interaction from an FM monolayer CrCl₃ for various stacking registries along the long-diagonal in (b). Three high-symmetry configurations are shown atop. The curves are plotted using Eqs. (S1) and (S2) in Supporting Information 1, whose stacking dependence in a full unit cell are shown in (d) and (e). $\mathbf{n} = \mathbf{z}$ is used in the CrCl₃ layer.

sufficiently large. Importantly, contrary to the original anisotropic term K_0^t that is fixed by the material, this effective anisotropic energy $K_{eff}(\mathbf{r})$, depending on not only the orientation of the FM order \mathbf{n} but also on the relative distance \mathbf{r} between the magnetic moments of the top and bottom layers, is highly tunable. With the former being controlled by an applied magnetic field and the latter by an interlayer relative shift [51], these couplings provide unique possibilities to manipulate AFM order.

The underlying physics of the interlayer interaction induced effective anisotropy becomes more evident when one considers the AFM sublattice precession dynamics, via generalizing directly Kittel's original derivation in the case of a uniform magnetic field to a staggered sublattice magnetic field [32]. For an FM substrate with $\mathbf{n} = \mathbf{z}$, the AFM resonance frequency and the ratio of the precession amplitudes between two sublattice are (c.f. Supporting Information 2)

$$\begin{aligned} \omega_{\pm}(\mathbf{r}) &= \gamma Z_{eff}(\mathbf{r}) \pm \gamma \{ [K_0 + \tau K_{eff}(\mathbf{r})] \\ &\quad [2J + K_0 + \tau K_{eff}(\mathbf{r})] \}^{1/2}, \\ \chi_{\pm}(\mathbf{r}) &= -1 - [K_0 + \tau K_{eff}(\mathbf{r})]/J \mp \{ [K_0 + \tau K_{eff}(\mathbf{r})] \\ &\quad [2J + K_0 + \tau K_{eff}(\mathbf{r})] \}^{1/2}/J, \end{aligned} \quad (3)$$

where γ is the gyromagnetic ratio and the superscript t is

omitted. These two (\pm) modes have opposite chiralities that the magnetization precesses circularly in opposite manners. It is evident that the effective anisotropic energy $K_{eff}(\mathbf{r})$ plays the same role as K_0 and can enhance the resonance frequency. Interestingly, with a typical small K_0 , a stable AFM order requires $\tau K_{eff}(\mathbf{r}) > 0$, i.e. $K_{eff}(\mathbf{r}) > 0$ stabilizes Néel order with $\tau = 1$ and vice versa. The effective Zeeman field $Z_{eff}(\mathbf{r})$ lifts the degeneracy of the two modes, and the low-energy mode vanishes at a critical field value, beyond which spin flop phase develops.

The effective fields arising from the interlayer magnetic interaction can be quantitatively estimated from the energy discrepancy of certain magnetic configurations (c.f. Figure 2a). In particular, the effective anisotropic energy related to the discrepancy of the sublattice field can be calculated from the energy difference of configurations with top AFM layers that have opposite magnetic orders (I and II configurations in Figure 2a), which gives $E_{II} - E_I = 4K_{eff}$. On the other hand, the effective Zeeman energy related to the average of the sublattice field can be measured by the one with top FM layers (III and IV configurations), which gives $E_{IV} - E_{III} = 4Z_{eff}$.

In the following, we illustrate our results with a concrete example of a magnetic heterobilayer composed of an AFM MnPS₃ and an FM CrCl₃, both of which have been experimentally reported in its monolayer form and have almost identical honeycomb lattice constants. MnPS₃ has a very weak anisotropic energy $K_0 \sim 0.002J$ [52] and has been verified to be lack of long-range AFM order in its monolayer form [53]. CrCl₃ crystal has weak in-plane anisotropy and its magnetic order can be tuned to out-of-plane by a small applied magnetic field, which is much weaker than the effective Zeeman field at the high-symmetry stackings [54]. For a commensurate honeycomb bilayer, the interlayer stacking order is characterized by a vector \mathbf{r} , which measures the inplane shift of a top Mn atom to a bottom Cr atom defined in a monolayer unit cell (c.f. Figure 2b).

Figure 2c shows the first-principles calculated effective anisotropic field (blue dots) and Zeeman field (red squares) along the long-diagonal of the unit cell, where there exist three high-symmetry configurations shown atop. At AB and BA stackings, where one of the AFM sublattice sits on top of the FM magnetic atom while the other is on top of the hollow center, the discrepancy of the interlayer magnetic interaction at the two sublattices is largest. Indeed, a strongest anisotropic field K_{eff} is found, reaching as high as $40K_0$. Meanwhile, their opposite signs reflect a strong coupling between the anisotropic field and stacking order. At AA stacking, where the A and B sublattices of the top and bottom layer align, the effective field from the two sublattice matches, resulting in a zero effective anisotropic energy. Different from the anisotropic field, the effective Zeeman field is always positive that aligns with the substrate FM

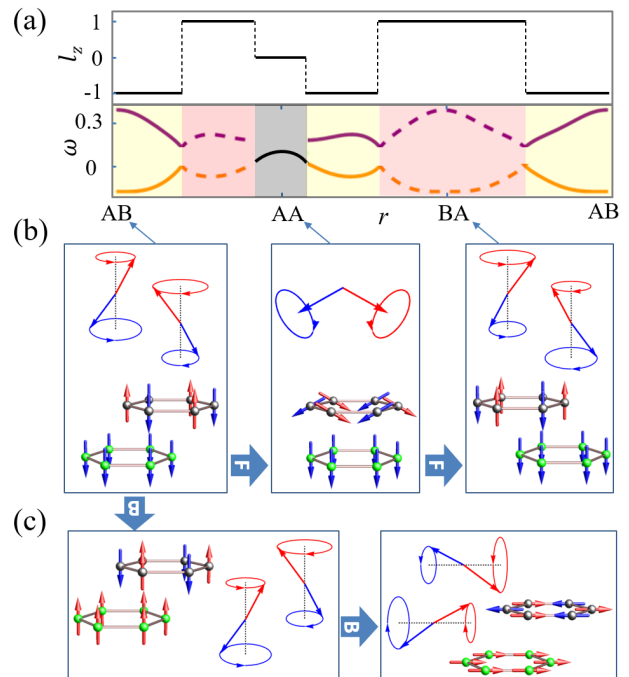


FIG. 3. (a) Stacking dependence of z -component of the Néel order $l_z = (m_A^z - m_B^z)/2$ (top) and AFM resonance frequency ω (bottom). The Néel order is flipped around the AB and BA regions, and vanishes around the AA region that enters into spin flop phase. The effective fields are adopted from Figure 2 with $\mathbf{n} = \mathbf{z}$. (b) Schematics of the precession of the AFM sublattice magnetization and its magnetic orientation for three high-symmetry configurations, which are related to each other via an interlayer shift between the layers exerted by a mechanical force (labeled by “F”). (c) A magnetic field (labeled by “B”) tuning the substrate FM order changes the AFM order in the top layer and its dynamics.

order, and approaches its maximum at AA stacking. Because the interlayer distance is much larger than the in-plane atomic variation in a unit cell, one can well fit the data using analytic expressions with low harmonic functions (c.f. curves in Figure 2c and see also Eqs. S(1) and S(2) in Supporting Information 1), whose variation in the whole unit cell are shown in Figures 2d and e [34, 55].

The coupling between the effective anisotropy field and interlayer stacking order suggests a mechanical way to control the AFM order and its dynamics by shifting relatively the two layers. The top panel of Figure 3a shows the z -component of Néel order as a function of interlayer translation, when the effective fields lie out of plane. Near the AB and BA stackings, a uniform AFM magnetization with $|l_z| = 1$ is developed but with an opposite sign, i.e. the Néel order flips, as schematically shown in Figure 3b. Near AA stacking, the strong Zeeman field together with weak anisotropy field destabilizes the AFM phase and favors a spin flop one with $l_z = 0$. The lower panel of Figure 3a shows the stacking dependence of AFM resonance frequency, which is largest at AB and BA stack-

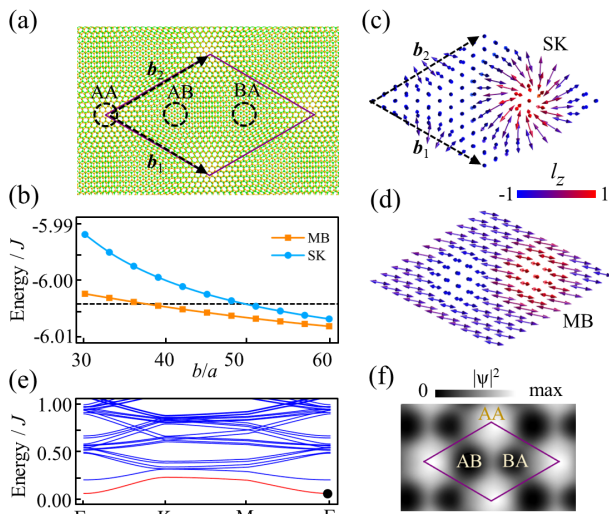


FIG. 4. (a) Schematics of a moiré superlattice with unit vectors $b_{1,2}$ formed by twisting a commensurate magnetic bilayer. (b) Energy per moiré cell as a function of moiré periodicity for AFM MB and SK textures, which are schematically shown in (c) and (d). The dashed line is the energy for uniform AFM state. The effective fields are adopted from Figure 2 with $\mathbf{n} = \mathbf{z}$. (e) Magnon miniband of an MB texture with $b = 42a$. (f) Wavefunction distribution of the lowest-energy magnon (black dot in (e)), which is localized around the AA region of a moiré.

ings, indicating their best magnetic stability. Because the effective Zeeman field is always positive, the lower-energy mode is always ω_- with a fixed chirality. At AB and BA stackings, although degenerate in energy, these two modes have opposite sublattice precession ratio because of the flipped Néel order (see Eq. (3)).

The coupling to the FM order of the substrate layer provides another magnetic way to control the AFM order and its dynamics (c.f. Figure 3c). Different from the mechanical control, which only flips the sign of the effective anisotropic field, reversing the FM order would flip the sign of the effective Zeeman field as well. In this case, the lower-energy mode changes from ω_- to ω_+ , which have opposite chiralities.

AFM textures in magnetic moiré superlattices.— The stacking dependent effective anisotropic field provides a unique possibility to engineer AFM textures [56] in moiré superlattice formed by a relative twist or strain between the commensurate heterobilayer (c.f. Figure 4a). The periodicity b of a moiré is inversely proportional to the misaligned angle and lattice mismatch, which can be further controlled by a twist or strain [57, 58]. Compared with nonmagnetic one [33–38, 42–45], a magnetic moiré, composed of lattices assigned with magnetic atoms, can be regarded as a superlattice of magnetic moments [59–65]. The smoothly changing atomic registry in a moiré then introduces a landscape of effective anisotropic and Zeeman fields for the top AFM layer. We assume that

the superlattice is formed by two rigid lattices so that there exists a linear mapping between local region in the moiré and registry-dependent commensurate stacking defined in a monolayer unit cell. We notice that when the substrate FM layer has a nonuniform magnetic texture, the effective field would also show a spatial dependence even for a commensurate atomic bilayer. This FM texture is possible when a weak out-of-plane magnetic field is applied to tune the initially in-plane magnetic order in the CrCl_3 layer.

In terms of a spatially varying field, the AFM monolayer in the magnetic moiré can be modeled by an AFM monolayer imposed with laterally modulated anisotropic and Zeeman fields,

$$H = \sum_{\langle i,j \rangle} J \mathbf{m}_i \mathbf{m}_j - [K_0 + K_{eff}(\mathbf{R}_i)] m_{z,i}^2 - Z_{eff}(\mathbf{R}_i) m_{z,i},$$

where \mathbf{R}_i is the atomic position in a moiré and we have assumed that the magnetization in the substrate layer is along \mathbf{z} -direction. The stable magnetic textures in a moiré can be obtained by relaxing from different initial magnetic configurations using Landau-Lifshitz-Gilbert equation [49, 66]. For a long-wavelength moiré, we find that the uniform AFM magnetization becomes unstable. Instead, magnetic textures, like AFM magnetic bubble (MB) and skyrmion (SK), become stable low-energy configurations (schematically shown in Figures 4c and d). With the increase of moiré periodicity, these AFM textures become more stable, as evidenced by the decrease in their energy (c.f. Figure 4b). Because SK has an inplane vortex structure, it costs more intralayer exchange energy and thus is energetically higher than MB. Interestingly, because these AFM textures are generated and stabilized by a landscape of the effective field, they can be driven by a slight interlayer shift and regulated by an external magnetic field, which provides new means to tune AFM textures (c.f. Supporting Information 3). These moiré generated AFM textures avoid the stringent requirement of Dzyaloshinskii-Moriya interaction [67], which can be utilized to engineer topological phases of various quasiparticles [68–70].

Usually the spatial modulation of the magnetic order in magnetic textures leads to low-energy magnons localized at domain walls [71]. Instead, in moiré magnetic textures, there exists an additional spatially modulated effective field (c.f. Supporting Information 4). This field landscape tends to localize low-energy magnons around the AA region, where the magnetization is most unstable. Figure 4e shows the calculated magnon miniband, where a low-energy band is separated from others. Its wavefunction is localized around AA region of a moiré (c.f. Figure 4f). When thermal fluctuation is considered, magnetic orders in these regions are more fragile than the ones in other regions.

Discussion and conclusions.—The effective anisotropic field that stabilizes AFM order arising from the interlayer

magnetic interaction is a general result in van der Waals magnets. A recent experimental study on van der Waals AFM MnPS₃ has shown that long-range magnetic order persists from bulk to bilayer, while absent in monolayer [53]. This is consistent with our result that interlayer magnetic interaction creates an effective anisotropy that stabilizes long-range magnetic order, while which is absent in the monolayer case without an interlayer interaction. For bilayer MnPS₃, our first-principles calculations show that the interlayer interaction induced effective anisotropic energy can reach as high as $12K_0$ (c.f. Supporting Information 5).

In summary, we have revealed a tunable strong magnetic anisotropy in van der Waals magnets that can stabilize and manipulate 2D AFM order. This magnetic anisotropy arises from a sublattice dependent interlayer magnetic interaction that strongly couples with the interlayer stacking order and magnetic order of the substrate layer. These couplings provide unprecedented mechanical and magnetic controls over AFM order as well as its dynamics. In the moiré of a magnetic heterostructure, the stacking dependent anisotropic field can be utilized to engineer nonuniform AFM textures, in which low-energy magnons are periodically trapped in the moiré. Our results point to a new route to explore and manipulate 2D AFM magnetism, with potential applications in constructing atomic-scale AFM spintronic devices and studying magnon condensation physics.

Supporting Information.—The Supporting Information includes details of the first-principles calculations, AFM magnetization dynamics, mechanical and magnetic control over the moiré AFM textures, localized magnons in moiré AFM textures, and effective anisotropic field in bilayer MnPS₃.

Acknowledgments.—We thank Wang Yao for stimulating discussions at initial stage of this work. This work is supported by the National Natural Science Foundation of China (11904095), the National Key Research and Development Program of Ministry of Science and Technology (2021YFA1200503), and the Fundamental Research Funds for the Central Universities from China.

* tongqj@hnu.edu.cn

- [1] Burch, K. S.; Mandrus, D.; Park, J.-G. Magnetism in two-dimensional van der Waals materials. *Nature* **2018**, *563*, 47-52.
- [2] Gong, C.; Zhang, X. Two-dimensional magnetic crystals and emergent heterostructure devices. *Science* **2019**, *363*, 706.
- [3] Mak, K. F.; Shan, J.; Ralph, D. C. Probing and controlling magnetic states in 2D layered magnetic materials. *Nat. Rev. Phys.* **2019**, *1*, 646-661.
- [4] Huang, B.; McGuire, M. A.; May, A. F.; Xiao, D.; Jarillo-Herrero, P.; Xu, X. Emergent phenomena and proximity effects in two-dimensional magnets and heterostructures. *Nat. Mater.* **2020**, *19*, 1276-1289.
- [5] Rahman, S.; Torres, J. F.; Khan, A. R.; Lu, Y. Recent Developments in van der Waals Antiferromagnetic 2D Materials: Synthesis, Characterization, and Device Implementation. *ACS Nano* **2021**, *15*, 17175-17213.
- [6] Gong, C.; Li, L.; Li, Z.; Ji, H.; Stern, A.; Xia, Y.; Cao, T.; Bao, W.; Wang, C.; Wang, Y.; Qiu, Z. Q.; Cava, R. J.; Louie, S. G.; Xia, J.; Zhang, X. Discovery of intrinsic ferromagnetism in two-dimensional van der Waals crystals. *Nature* **2017**, *546*, 265-269.
- [7] Huang, B.; Clark, G.; Navarro-Moratalla, E.; Klein, D. R.; Cheng, R.; Seyler, K. L.; Zhong, D.; Schmidgall, E.; McGuire, M. A.; Cobden, D. H.; Yao, W.; Xiao, D.; Jarillo-Herrero, P.; Xu, X. Layer-dependent ferromagnetism in a van der Waals crystal down to the monolayer limit. *Nature* **2017**, *546*, 270-273.
- [8] Jiang, S.; Shan, J.; Mak, K. F. Electric-field switching of two-dimensional van der Waals magnets. *Nat. Mater.* **2018**, *17*, 406-410.
- [9] Huang, B.; Clark, G.; Klein, D. R.; MacNeill, D.; Navarro-Moratalla, E.; Seyler, K. L.; Wilson, N.; McGuire, M. A.; Cobden, D. H.; Xiao, D.; Yao, W.; Jarillo-Herrero, P.; Xu, X. Electrical control of 2D magnetism in bilayer CrI₃. *Nat. Nanotechnol.* **2018**, *13*, 544-548.
- [10] Wang, Z.; Zhang, T.; Ding, M.; Dong, B.; Li, Y.; Chen, M.; Li, X.; Huang, J.; Wang, H.; Zhao, X.; Li, Y.; Li, D.; Jia, C.; Sun, L.; Guo, H.; Ye, Y.; Sun, D.; Chen, Y.; Yang, T.; Zhang, J.; Ono, S.; Han, Z.; Zhang, Z. Electric-field control of magnetism in a few-layered van der Waals ferromagnetic semiconductor. *Nat. Nanotechnol.* **2018**, *13*, 554-559.
- [11] Deng, Y.; Yu, Y.; Song, Y.; Zhang, J.; Wang, N. Z.; Sun, Z.; Yi, Y.; Wu, Y. Z.; Wu, S.; Zhu, J.; Wang, J.; Chen, X. H.; Zhang, Y. Gate-tunable room-temperature ferromagnetism in two-dimensional Fe₃GeTe₂. *Nature* **2018**, *563*, 94-99.
- [12] Song, T.; Cai, X.; Tu, M. W.-Y.; Zhang, X.; Huang, B.; Wilson, N. P.; Seyler, K. L.; Zhu, L.; Taniguchi, T.; Watanabe, K.; McGuire, M. A.; Cobden, D. H.; Xiao, D.; Yao, W.; Xu, X. Giant tunneling magnetoresistance in spin-filter van der Waals heterostructures. *Science* **2018**, *360*, 1214-1218.
- [13] Klein, D. R.; MacNeill, D.; Lado, J. L.; Soriano, D.; Navarro-Moratalla, E.; Watanabe, K.; Taniguchi, T.; Manni, S.; Canfield, P.; Fernández-Rossier, J.; Jarillo-Herrero, P. Probing magnetism in 2D van der Waals crystalline insulators via electron tunneling. *Science* **2018**, *360*, 1218-1222.
- [14] Wang, Z.; Gutiérrez-Lezama, I.; Ubrig, N.; Kroner, M.; Gibertini, M.; Taniguchi, T.; Watanabe, K.; Imamoglu, A.; Giannini, E.; Morpurgo, A. F. Very large tunneling magnetoresistance in layered magnetic semiconductor CrI₃. *Nat. Commun.* **2018**, *9*, 2516.
- [15] Cenker, J.; Huang, B.; Suri, N.; Thijssen, P.; Miller, A.; Song, T.; Taniguchi, T.; Watanabe, K.; McGuire, M. A.; Xiao, D.; Xu, X. Direct observation of two-dimensional magnons in atomically thin CrI₃. *Nat. Phys.* **2021**, *17*, 20-25.
- [16] Wang, X.; Du, K.; Liu, Y. Y. F.; Hu, P.; Zhang, J.; Zhang, Q.; Owen, M. H. S.; Lu, X.; Gan, C. K.; Sengupta, P.; Kloc, C.; Xiong, Q. Raman spectroscopy of atomically thin two-dimensional magnetic iron phosphorus trisulfide (FePS₃) crystals. *2D Mater.* **2016**, *3*,

- 031009.
- [17] Du, K.-Z.; Wang, X.-Z.; Liu, Y.; Hu, P.; Utama, M. I. B.; Gan, C. K.; Xiong, Q.; Kloc, C. Weak Van der Waals Stacking, Wide-Range Band Gap, and Raman Study on Ultrathin Layers of Metal Phosphorus Trichalcogenides. *ACS Nano* **2016**, *10*, 1738-1743.
- [18] Lee, J.-U.; Lee, S.; Ryoo, J. H.; Kang, S.; Kim, T. Y.; Kim, P.; Park, C.-H.; Park, J.-G.; Cheong, H. Ising-Type Magnetic Ordering in Atomically Thin FePS₃. *Nano Lett.* **2016**, *16*, 7433-7438.
- [19] Kim, K.; Lim, S. Y.; Kim, J.; Lee, J.-U.; Lee, S.; Kim, P.; Park, K.; Son, S.; Park, C.-H.; Park, J.-G.; Cheong, H. Antiferromagnetic ordering in van der Waals 2D magnetic material MnPS₃ probed by Raman spectroscopy. *2D Mater.* **2019**, *6*, 041001.
- [20] Kang, S.; Kim, K.; Kim, B. H.; Kim, J.; Sim, K. I.; Lee, J.-U.; Lee, S.; Park, K.; Yun, S.; Kim, T.; Nag, A.; Walters, A.; Garcia-Fernandez, M.; Li, J.; Chapon, L.; Zhou, K.-J.; Son, Y.-W.; Kim, J. H.; Cheong, H.; Park, J.-G. Coherent many-body exciton in van der Waals antiferromagnet NiPS₃. *Nature* **2020**, *583*, 785-789.
- [21] Wang, X.; Cao, J.; Lu, Z.; Cohen, A.; Kitadai, H.; Li, T.; Tan, Q.; Wilson, M.; Lui, C. H.; Smirnov, D.; Sharifzadeh, S.; Ling, X. Spin-induced linear polarization of photoluminescence in antiferromagnetic van der Waals crystals. *Nat. Mater.* **2021**, *20*, 964-970.
- [22] Ni, Z.; Haglund, A. V.; Wang, H.; Xu, B.; Bernhard, C.; Mandrus, D. G.; Qian, X.; Mele, E. J.; Kane, C. L.; Wu, L. Imaging the Néel vector switching in the monolayer antiferromagnet MnPSe₃ with strain-controlled Ising order. *Nat. Nanotechnol.* **2021**, *16*, 782-787.
- [23] Hwangbo, K.; Zhang, Q.; Jiang, Q.; Wang, Y.; Fonseca, J.; Wang, C.; Diederich, G. M.; Gamelin, D. R.; Xiao, D.; Chu, J.-H.; Yao, W.; Xu, X. Highly anisotropic excitons and multiple phonon bound states in a van der Waals antiferromagnetic insulator. *Nat. Nanotechnol.* **2021**, *16*, 655-660.
- [24] Kampfrath, T.; Sell, A.; Klatt, G.; Pashkin, A.; Mährlein, S.; Dekorsy, T.; Wolf, M.; Fiebig, M.; Leitenstorfer, A.; Huber, R. Coherent terahertz control of antiferromagnetic spin waves. *Nat. Photon.* **2011**, *5*, 31-34.
- [25] Cheng, R.; Xiao, J.; Niu, Q.; Brataas, A. Spin Pumping and Spin-Transfer Torques in Antiferromagnets. *Phys. Rev. Lett.* **2014**, *113*, 057601.
- [26] Rezende, S. M.; Azevedo, A.; Rodríguez-Suárez, R. L. Introduction to antiferromagnetic magnons. *J. Appl. Phys.* **2019**, *126*, 151101.
- [27] Xing, W.; Qiu, L.; Wang, X.; Yao, Y.; Ma, Y.; Cai, R.; Jia, S.; Xie, X. C.; Han, W. Magnon Transport in Quasi-Two-Dimensional van der Waals Antiferromagnets. *Phys. Rev. X* **2019**, *9*, 011026.
- [28] Li, J.; Wilson, C. B.; Cheng, R.; Lohmann, M.; Kavand, M.; Yuan, W.; Aldosary, M.; Agladze, N.; Wei, P.; Sherwin, M. S.; Shi, J. Spin current from sub-terahertz-generated antiferromagnetic magnons. *Nature* **2020**, *578*, 70-74.
- [29] Jungwirth, T.; Marti, X.; Wadley, P.; Wunderlich, J. Antiferromagnetic spintronics. *Nat. Nanotechnol.* **2016**, *11*, 231-241.
- [30] Jungwirth, T.; Sinova, J.; Manchon, A.; Marti, X.; Wunderlich, J.; Felser, C. The multiple directions of antiferromagnetic spintronics. *Nat. Phys.* **2018**, *14*, 200-203.
- [31] Mermin, N. D.; Wagner, H. Absence of Ferromagnetism or Antiferromagnetism in One- or Two-Dimensional Isotropic Heisenberg Models. *Phys. Rev. Lett.* **1966**, *17*, 1133.
- [32] Kittel, C. Theory of Antiferromagnetic Resonance. *Phys. Rev.* **1951**, *82*, 565.
- [33] Zhang, C.; Chuu, C.-P.; Ren, X.; Li, M.-Y.; Li, L.-J.; Jin, C.; Chou, M.-Y.; Shih, C.-K. Interlayer couplings, Moiré patterns, and 2D electronic superlattices in MoS₂/WSe₂ hetero-bilayers. *Sci. Adv.* **2017**, *3*, e1601459.
- [34] Tong, Q.; Yu, H.; Zhu, Q.; Wang, Y.; Xu, X.; Yao, W. Topological mosaics in moiré superlattices of van der Waals heterobilayers. *Nat. Phys.* **2017**, *13*, 356-362.
- [35] Seyler, K. L.; Rivera, P.; Yu, H.; Wilson, N. P.; Ray, E. L.; Mandrus, D. G.; Yan, J.; Yao, W.; Xu, X. Signatures of moiré-trapped valley excitons in MoSe₂/WSe₂ heterobilayers. *Nature* **2019**, *567*, 66-70.
- [36] Tran, K.; Moody, G.; Wu, F.; Lu, X.; Choi, J.; Kim, K.; Rai, A.; Sanchez, D. A.; Quan, J.; Singh, A.; Embley, J.; Zepeda, A.; Campbell, M.; Autry, T.; Taniguchi, T.; Watanabe, K.; Lu, N.; Banerjee, S. K.; Silverman, K. L.; Kim, S.; Tutuc, E.; Yang, L.; MacDonald, A. H.; Li, X. Evidence for moiré excitons in van der Waals heterostructures. *Nature* **2019**, *567*, 71-75.
- [37] Jin, C.; Regan, E. C.; Yan, A.; Utama, M. I. B.; Wang, D.; Zhao, S.; Qin, Y.; Yang, S.; Zheng, M.; Shi, S.; Watanabe, K.; Taniguchi, T.; Tongay, S.; Zettl, A.; Wang, F. Observation of moiré excitons in WSe₂/WS₂ heterostructure superlattices. *Nature* **2019**, *567*, 76-80.
- [38] Alexeev, E. M.; Ruiz-Tijerina, D. A.; Danovich, M.; Hamer, M. J.; Terry, D. J.; Nayak, P. K.; Ahn, S.; Pak, S.; Lee, J.; Sohn, J. I.; Molas, M. R.; Koperski, M.; Watanabe, K.; Taniguchi, T.; Novoselov, K. S.; Gorbatchev, R. V.; Shin, H. S.; Fal'ko, V. I.; Tartakovskii, A. I. Resonantly hybridized excitons in moiré superlattices in van der Waals heterostructures. *Nature* **2019**, *567*, 81-86.
- [39] Song, T.; Fei, Z.; Yankowitz, M.; Lin, Z.; Jiang, Q.; Hwangbo, K.; Zhang, Q.; Sun, B.; Taniguchi, T.; Watanabe, K.; McGuire, M. A.; Graf, D.; Cao, T.; Chu, J.-H.; Cobden, D. H.; Dean, C. R.; Xiao, D.; Xu, X. Switching 2D magnetic states via pressure tuning of layer stacking. *Nat. Mater.* **2019**, *18*, 1298-1302.
- [40] Li, T.; Jiang, S.; Sivadas, N.; Wang, Z.; Xu, Y.; Weber, D.; Goldberger, J. E.; Watanabe, K.; Taniguchi, T.; Fennie, C. J.; Mak, K. F.; Shan, J. Pressure-controlled interlayer magnetism in atomically thin CrI₃. *Nat. Mater.* **2019**, *18*, 1303-1308.
- [41] Chen, W.; Sun, Z.; Wang, Z.; Gu, L.; Xu, X.; Wu, S.; Gao, C. Direct observation of van der Waals stacking dependent interlayer magnetism. *Science* **2019**, *366*, 983-987.
- [42] Enaldiev, V. V.; Zólyomi, V.; Yelgel, C.; Magorrian, S. J.; Fal'ko, V. I. Stacking Domains and Dislocation Networks in Marginally Twisted Bilayers of Transition Metal Dichalcogenides. *Phys. Rev. Lett.* **2020**, *124*, 206101.
- [43] Stern, M. V.; Waschitz, Y.; Cao, W.; Nevo, I.; Watanabe, K.; Taniguchi, T.; Sela, E.; Urbakh, M.; Hod, O.; Shalom, M. B. Interfacial ferroelectricity by van der Waals sliding. *Science* **2021**, *372*, 1462-1466.
- [44] Yasuda, K.; Wang, X.; Watanabe, K.; Taniguchi, T.; Jarillo-Herrero, P. Stacking-engineered ferroelectricity in bilayer boron nitride. *Science* **2021**, *372*, 1458-1462.
- [45] Woods, C. R.; Ares, P.; Nevison-Andrews, H.; Holwill, M. J.; Fabregas, R.; Guinea, F.; Geim, A. K.; Novoselov,

- K. S.; Walet, N. R.; Fumagalli L. Charge-polarized interfacial superlattices in marginally twisted hexagonal boron nitride. *Nat. Commun.* **2021**, *12*, 347.
- [46] Kennes, D. M.; Claassen, M.; Xian, L.; Georges, A.; Millis, A. J.; Hone, J.; Dean, C. R.; Basov, D. N.; Pasupathy, A. N.; Rubio, A. Moiré heterostructures as a condensed-matter quantum simulator. *Nat. Phys.* **2021**, *17*, 155-163.
- [47] Andrei, E. Y.; Efetov, D. K.; Jarillo-Herrero, P.; MacDonald, A. H.; Mak, K. F.; Senthil, T.; Tutuc, E.; Yazdani, A.; Young, A. F. The marvels of moiré materials. *Nat. Rev. Mater.* **2021**, *6*, 201-206.
- [48] Wilson, N. P.; Yao, W.; Shan, J.; Xu, X. Excitons and emergent quantum phenomena in stacked 2D semiconductors. *Nature* **2021**, *599*, 383-392.
- [49] Landau, L. D.; Lifshitz, E. M. On the Theory of the Dispersion of Magnetic Permeability in Ferromagnetic Bodies. *Phys. Z. Sowjetunion* **1953**, *8*, 153-164.
- [50] Berkowitz, A. E.; Takano, K. Exchange anisotropy—a review. *J. Magn. Magn. Mater.* **1999**, *200*, 552-570.
- [51] Jiang, L.; Wang, S.; Shi, Z.; Jin, C.; Utama, M. I. B.; Zhao, S.; Shen, Y.-R.; Gao, H.-J.; Zhang, G.; Wang, F. Manipulation of domain-wall solitons in bi- and trilayer graphene. *Nat. Nanotechnol.* **2018**, *13*, 204-208.
- [52] Okuda, K.; Kurosawa, K.; Saito, S.; Honda, M.; Yu, Z.; Date, M. Magnetic Properties of Layered Compound MnPS₃. *J. Phys. Soc. Jpn.* **1986**, *55*, 4456-4463.
- [53] Ni, Z.; Zhang, H.; Hopper, D. A.; Haglund, A. V.; Huang, N.; Jariwala, D.; Bassett, L. C.; Mandrus, D. G.; Mele, E. J.; Kane, C. L.; Wu, L. Direct Imaging of Antiferromagnetic Domains and Anomalous Layer-Dependent Mirror Symmetry Breaking in Atomically Thin MnPS₃. *Phys. Rev. Lett.* **2021**, *127*, 187201.
- [54] McGuire, M. A.; Clark, G.; KC, S.; Chance, W. M.; Jellison, G. E., Jr.; Cooper, V. R.; Xu, X.; Sales, B. C. Magnetic behavior and spin-lattice coupling in cleavable van der Waals layered CrCl₃ crystals. *Phys. Rev. Mater.* **2017**, *1*, 014001.
- [55] Jung, J.; Raoux, A.; Qiao, Z.; MacDonald, A. H. *Ab initio* theory of moiré superlattice bands in layered two-dimensional materials. *Phys. Rev. B* **2014**, *89*, 205414.
- [56] Gomonay, O.; Baltz, V.; Brataas, A.; Tserkovnyak, Y. Antiferromagnetic spin textures and dynamics. *Nat. Phys.* **2018**, *14*, 213-216.
- [57] Ribeiro-Palau, R.; Zhang, C.; Watanabe, K.; Taniguchi, T.; Hone, J.; Dean, C. R. Twistable electronics with dynamically rotatable heterostructures. *Science* **2018**, *361*, 690-693.
- [58] Bai, Y.; Zhou, L.; Wang, J.; Wu, W.; McGilly, L.; Halbertal, D.; Lo, C. F. B.; Liu, F.; Ardelean, J.; Rivera, P.; Finney, N. R.; Yang, X.-C.; Basov, D. N.; Yao, W.; Xu, X.; Hone, J.; Pasupathy, A. N.; Zhu, X.-Y. Excitons in strain-induced one-dimensional moiré potentials at transition metal dichalcogenide heterojunctions. *Nat. Mater.* **2020**, *19*, 1068-1073.
- [59] Tong, Q.; Liu, F.; Xiao, J.; Yao, W. Skyrmions in the Moiré of van der Waals 2D Magnets. *Nano Lett.* **2018**, *18*, 7194-7199.
- [60] Sivadas, N.; Okamoto, S.; Xu, X.; Fennie, C. J.; Xiao, D. Stacking-Dependent Magnetism in Bilayer CrI₃. *Nano Lett.* **2018**, *18*, 7658-7664.
- [61] Hejazi, K.; Luo, Z.-X.; Balents, L. Noncollinear phases in moiré magnets. *Proc. Natl. Acad. Sci. U.S.A.* **2020**, *117*, 10721-10726.
- [62] Akram, M.; LaBollita, H.; Dey, D.; Kapeghian, J.; Erten, O.; Botana, A. S. Moiré skyrmions and chiral magnetic phases in twisted CrX₃ (X=I, Br, and Cl) bilayers. *Nano Lett.* **2021**, *21*, 6633-6639.
- [63] Song, T.; Sun, Q.-C.; Anderson, E.; Wang, C.; Qian, J.; Taniguchi, T.; Watanabe, K.; McGuire, M. A.; Stöhr, R.; Xiao, D.; Cao, T.; Wrachtrup, J.; Xu, X. Direct visualization of magnetic domains and moiré magnetism in twisted 2D magnets. *Science* **2021**, *374*, 1140-1144.
- [64] Xu, Y.; Ray, A.; Shao, Y.-T.; Jiang, S.; Lee, K.; Weber, D.; Goldberger, J. E.; Watanabe, K.; Taniguchi, T.; Muller, D. A.; Mak, K. F.; Shan, J. Coexisting ferromagnetic-antiferromagnetic state in twisted bilayer CrI₃. *Nat. Nanotechnol.* **2022**, *17*, 143-147.
- [65] Xie, H.; Luo, X.; Ye, G.; Ye, Z.; Ge, H.; Sung, S. H.; Rennich, E.; Yan, S.; Fu, Y.; Tian, S.; Lei, H.; Hovden, R.; Sun, K.; He, R.; Zhao, L. Twist engineering of the two-dimensional magnetism in double bilayer chromium triiodide homostructures. *Nature Physics* **2022**, *18*, 30-36.
- [66] Gilbert, T. L. A phenomenological theory of damping in ferromagnetic materials. *IEEE Trans. Magn.* **2004**, *40*, 3443-3449.
- [67] Zhang, X.; Zhou, Y.; Ezawa, M. Antiferromagnetic skyrmion: stability, creation and manipulation. *Sci. Rep.* **2016**, *6*, 24795.
- [68] Göbel, B.; Mook, A.; Henk, J.; Mertig, I. Antiferromagnetic skyrmion crystals: Generation, topological Hall, and topological spin Hall effect. *Phys. Rev. B* **2017**, *96*, 060406(R).
- [69] Díaz, S. A.; Klinovaja, J.; Loss, D. Topological magnons and edge states in antiferromagnetic skyrmion crystals. *Phys. Rev. Lett.* **2019**, *122*, 187203.
- [70] Díaz, S. A.; Klinovaja, J.; Loss, D.; Hoffman, S. Majorana bound states induced by antiferromagnetic skyrmion textures. *Phys. Rev. B* **2021**, *104*, 214501.
- [71] Yu, H.; Xiao, J.; Schultheiss, H. Magnetic texture based magnonics. *Phys. Rep.* **2021**, *905*, 1-59.